Enhanced Electrical Conductivity and Interlaminar Fracture Toughness of CF/EP Composites via Interleaving Conductive Thermoplastic Films

Jialiang Liu[1] · Yuntao Li[1] · Dong Xiang[1] (ORCID) · Chunxia Zhao[1] · Bin Wang[1] · Hui Li[1]

Abstract

The poor electrical conductivity and interlaminar fracture toughness of carbon fiber reinforced epoxy (CF/EP) composites could reduce their reliability for aerospace applications. In this work, multi-walled carbon nanotubes (MWCNTs) doped polyethersulfone (PES) conductive thermoplastic films (CTFs) were prepared by solution casting method. The as-obtained composites were then interleaved into CF/EP prepregs to yield composite laminates. The effects of CTFs on the electrical conductivity and interlaminar fracture toughness of the as-prepared CF/EP composites were investigated. The results suggested an increase in conductivity of laminates by 104% and 84% in the transverse (Y) and through-thickness (Z) directions, respectively. The Mode I and Mode II interlaminar fracture toughness values were evaluated by double cantilever beam (DCB) and end-notched flexure (ENF) testing. The data revealed that the introduction of CTFs with 10wt% MWCNTs led to enhancement in Mode I and Mode II interlaminar fracture toughness of Composite laminates by 206% and 47%, respectively. The failure mechanism was investigated through microstructural and morphological changes in the composites studied by scanning electron microscopy (SEM). This work provides valuable guidance for the simultaneous enhancement of electrical conductivity and interlaminar fracture toughness of CF/EP composites.

Keywords CF / EP composites · Interlaminar fracture toughness · Conductivity · Carbon nanotubes · Polyethersulfone

1 Introduction

In recent decades, carbon fiber reinforced composites have gradually replaced the traditional metal-based materials in the aerospace industry owing to their high specific strength, superior stiffness, and good fatigue and corrosion resistance. For instance, carbon fiber

✉ Yuntao Li
yuntaoli@swpu.edu.cn

✉ Dong Xiang
dxiang01@hotmail.com

1   School of New Energy and Materials, Southwest Petroleum University, Chengdu 610500, China

reinforced composites(CFRP) are used in parts constituting the Airbus A350, Airbus A380, and Boeing 787 [1, 2]. Moreover, carbon fiber reinforced composites possess light-weight than metal-based materials, thereby saving fuel consumption and economic costs. However, the electrical conductivity remains a crucial problem in the aerospace industry. Though carbon fiber itself has good electrical conductivity, it still not good enough for use in the aerospace industry when compared to metal-based materials like aluminum and copper [3, 4]. Therefore, the development of novel conductive structures with good conductivity is highly desirable in the aerospace industry.

In the last few years, numerous conductive nanoparticles have been added to matrices to build novel structures with improved conductivities to meet the requirements of the aerospace industry. Examples include silver nanowires [5], graphene [6], carbon black [7], and carbon nanotubes (CNTs) [8–10]. Notably, CNTs have so far been demonstrated as one of the best conductive fillers for conductive polymers due to their excellent mechanical and physical properties, such as high strength, specific modulus, and superior electrical conductivity [11, 12]. However, the high aspect ratio and van der Waals force in CNTs often lead to excessive aggregation, thereby affecting their comprehensive properties in various materials [8].

On the other hand, the structures of composite materials used in aircraft are very sensitive to low-speed impact of birds, hail, among other phenomena. These would deteriorate the performance of composite materials and affect safety [13, 14]. Furthermore, different composite materials possess various properties, which will dictate the type of damage during manufacturing and use. Examples include delamination, crack formation, surface scratching, size of pores, and degumming [15]. Among these, delamination is the primary mode of failure often caused by the growth of crack formation in the matrix under the action of an external force. The growth of delamination is mainly driven by the interlaminar shear stress induced by bending of laminates during impact [16, 17]. Such delamination phenomena are mainly generated by loading conditions of Mode I and Mode II of formed cracks under common loads, such as impact and fatigue[16–18].

Therefore, various studies have so far been carried out to improve the interlayer properties and performances of composite materials through Z-pins [19], three-dimensional weaving [20, 21], thickness stitching [22], and interleaf modification [23]. Among these, interlayer modification is relevant for inserting composite films into interlayers of carbon fiber to improve the mechanical and or electrical properties [24].

In recent years, interlayer materials have been inserted into carbon fiber reinforced composites to improve mechanical and electrical properties. This has been achieved through several methods, such as nanofiber veils [4, 25, 26], nanoparticles [3, 27], and thermoplastic films [24, 28]. Various factors have been shown to affect the interlaminar toughness of composite materials. Among these, inhibiting the fracture of fiber bundle, as well as crack growth have been pointed out as important factors enhance interlaminar fracture toughness. Therefore, the selection of proper interface reinforcement materials should be considered as an important factor for enhancing the interfacial forces.

Polyethersulfone (PES) is a typical thermoplastic toughening material with good chemical and physical compatibility in thermosetting resins [29]. The fracture toughness of composite materials can significantly be improved by inserting PES interleaf between laminated plates [30–32]. For instance, Mimura et al. [33] added 10 wt% PES to biphenyl epoxy resin and recorded an increase in fracture toughness and glass transition temperature (Tg) by respectively 60% and 20% when compared to unmodified resin. Zheng et al. [27] introduced 10 wt% dissolvable PES fiber as an interlaminar layer and noticed improvement in Mode I fracture toughness energy of the composites by

five-fold when compared to the control specimen. Cheng et al. [34] incorporated inter-leaved with uniformly aligned PES fiber webs into laminated plates and observed maximum enhancement in Mode I and II fracture toughness energies of the composites by 120% and 68.8% when compared to those without interleaves, respectively.

Though these research methods might increase the toughness and/or conductivity of composite materials to some extent, they still suffer from several drawbacks like complex processing, difficult to control, unsuitable for industrial production, and high cost. Moreover, composite materials used in the aerospace industry must satisfy good conductivity and mechanical properties simultaneously.

In sum, selected methods should not only conform to the actual manufacturing process but also maximize the production value to improve the comprehensive properties of composite materials. In this work, the electrical and mechanical properties of CF/EP composites were greatly enhanced by interlaminar toughening technology. First, composite film consisting of MWCNTs doped PES was manufactured through a simple solution casting method, and its electrical properties were tested to evaluate its suitability. Next, conductive PES film was inserted into CF/EP prepreg layer, and composite laminate was obtained by hot pressing. The mechanical and electrical properties of the as-obtained composites were then tested, and micromorphological and fracture mechanisms were determined. The results showed significant increases in both electrical conductivity and interlaminar fracture toughness of the modified CF/EP composites.

1.1 Experimental

1.1.1 Materials

MWCNTs (NANOCYL NC7000) with an average length of 1.5 nm, a diameter of 9.5 mm, and a density of 2.0 g cm^{-3} were obtained from Nanocyl S.A. (Sambreville, Belgium). Unidirectional CF/EP prepregs (B-228H) were purchased from BONAT-ECH Advanced Materials Company (Beijing, China), and their physical and mechanical properties are summarized in Table 1. PES powder (Basf E1010) with a density of 1.37 g cm^{-3} was supplied by BASF Germany. N, N-Dimethylformamide (DMF) was provided by Kelong Chemical Reagent Company (Chengdu, China).

Table 1　Specifications of unidirectional CF/EP prepregs

Parameter Specification	
Carbon fiber model	T700
Fiber mass per unit area (g / m^2)	132±4
Resin content (wt%)	35±2
Monolayer prepreg thickness (mm)	0.125
Epoxy resin model	E1010
Tg of epoxy resin (°C)	225
Tensile strength in fiber direction (MPa)	2500
Bending strength (MPa)	1650

1.1.2 Fabrication of CTFs

CTFs with different MWCNTs contents (0, 0.2, 0.3, 0.5, 1, 3, 5, 7, 10, 15, and 20 wt%) were manufactured through solution casting method. First, multi-walled carbon nanotubes (MWCNTs) were added to DMF solution under constant stirring sonication for 30 min. Next, PES powder was added to MWCNTs/DMF suspension under sonication for 30 min followed by vigorous stirring at 160 ℃ for 2.5 h. Finally, MWCNTs/PES/DMF mixed solution was poured into a glass mold (150 mm×150 mm×8 mm) and left to dry at 80 ℃ for 12 h. The thickness of the as-produced CTFs ranged from 14 to 15 µm. The fabrication process of CTFs is displayed in Fig. 1.

1.1.3 Fabrication of CF/EP Composite Laminates and Specimens Testing

The unidirectional prepregs were first cut into square sheets of 150×150 mm size, and then twenty-four layers of prepregs were manually stacked as ply-by-ply in $[0°]_{24}$ for Mode I interlaminar and II fracture toughness testing. A layer of CTF was inserted between the 12th and 13th prepregs during manual layering. Furthermore, PTFE film (13 µm thick) coated with the released agent was inserted as a pre-crack, in which pre-crack length of Mode I was set to 50 mm and that of Mode II was 45 mm. Meanwhile, other unidirectional prepregs were cut into square sheets with size of 50×50 mm. A total of these twelve layers of prepregs were manually stacked as ply-by-ply in $[0°]_{12}$ for conductivity testing. A conductive film (a total of eleven CTFs) was inserted between each layer of prepreg.

After layup, the fabricated specimens were subjected to hot press curing process. To this end, two Teflon films were placed on the surface of a steel mold to facilitate the removal of the cured laminate. Finally, the composite laminates were naturally cooled to room temperature under 10 MPa pressure. The fabrication process of composite laminates is also shown in Fig. 1. The prepreg curing process of the composite laminates is depicted in Fig. 2.

For interlaminar fracture toughness testing of composite laminates, the average thickness of each specimen is about 4 mm. For electrical properties testing, the average thickness of each specimen is about 1.5 mm. The test samples were cut from the cured laminates using a water jet cutter. The size of samples subjected to fracture toughness testing was
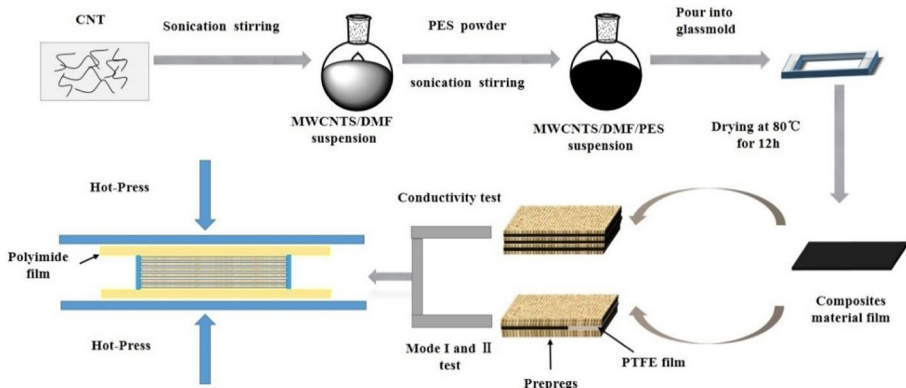

Fig. 1 Fabrication process of CTFs and CTF interleaved CF/EP composite laminates
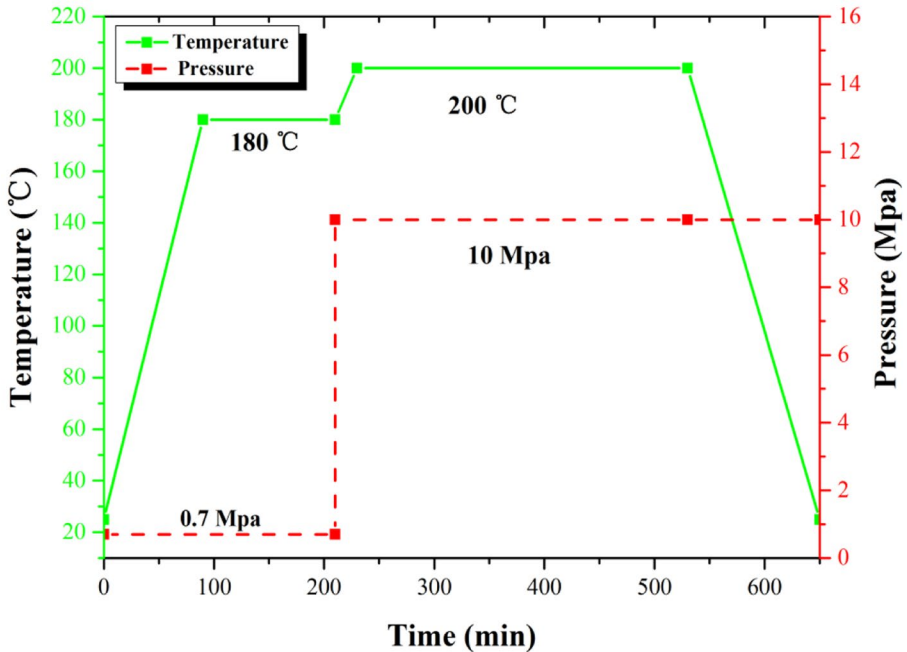
Fig. 2 Prepreg curing process of composite laminates

150 mm×20 mm×4 mm, and that for electrical properties was 12 mm×12 mm×1.5 mm. The dimensions of test samples are presented in Fig. 3.

1.1.4 Characterization

1.1.5 Microscopy

The conductive networks in the CTFs, as well as the fracture surface morphologies of DCB and ENF samples were observed by FEI Quanta 650 FEG field emission scanning electron microscopy at accelerating voltage of 30 kV. To emit abundant secondary electrons on the surfaces and facilitate the morphological identification, all specimens surfaces were sprayed with gold before any observation. Note that CTFs were etched in DMF solution before testing the conductive networks.

1.1.6 Electrical Conductivity

The values of volume conductivity of CTFs were measured at room temperature by two-point probe method and DC power supply voltage of 1 V. The CTFs were cut into rectangular strips with size of 40 mm×10 mm, and distance between electrodes was fixed to 30 mm. The conductivity of each prepared CF/EP laminate at room temperature was measured by a KEITHLEY 2000 multimeter using the four-wire method. The conductivities of composite laminates with dimension of 12 mm×12 mm×1.5 mm were also measured.
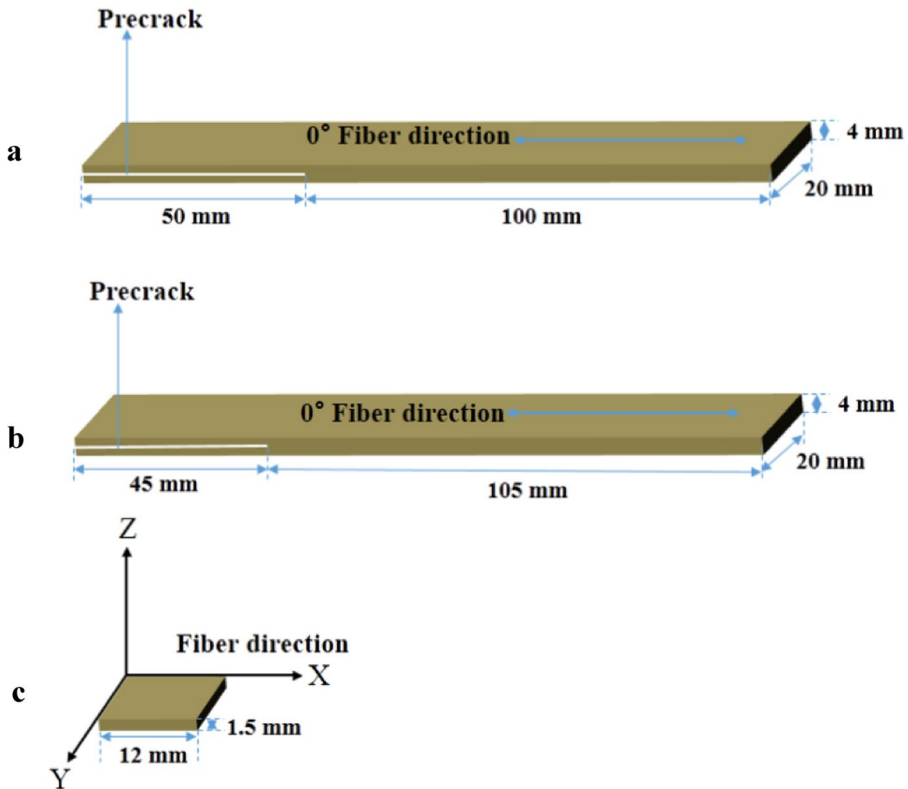
Fig. 3 Dimensions of different test samples: (**a**) Mode I test samples, (**b**) Mode II test samples, and (**c**) electrical performance test samples

Due to anisotropy of the fiber, the electrical conductivity was measured in three directions (fiber, transverse, and through-thickness directions), as shown in Fig. 4a. To reduce errors, all conductivity test samples were carried out at least three times. For testing, the specimen surface was first sanded with sandpaper and then cleaned with acetone and air-dried. Finally, the test surface was coated with a layer of conductive silver paste to minimize the contact resistance. The conductivity (S) values of CTFs and CF/EP laminates were calculated according to Eq. (1):

$$\sigma = \frac{L}{RA} \tag{1}$$

where, R, A and L represent the volume resistance, cross-sectional area and length of the specimen, respectively. Note that L and A represent the different geometric dimensions of the specimen when measured in three directions.

1.1.7 Mode I Interlaminar Fracture Toughness Testing

The Mode I interlayer fracture toughness of each composite laminate was tested by the double-cantilever-beams (DCB) test method (ASTM D5528). A universal testing machine
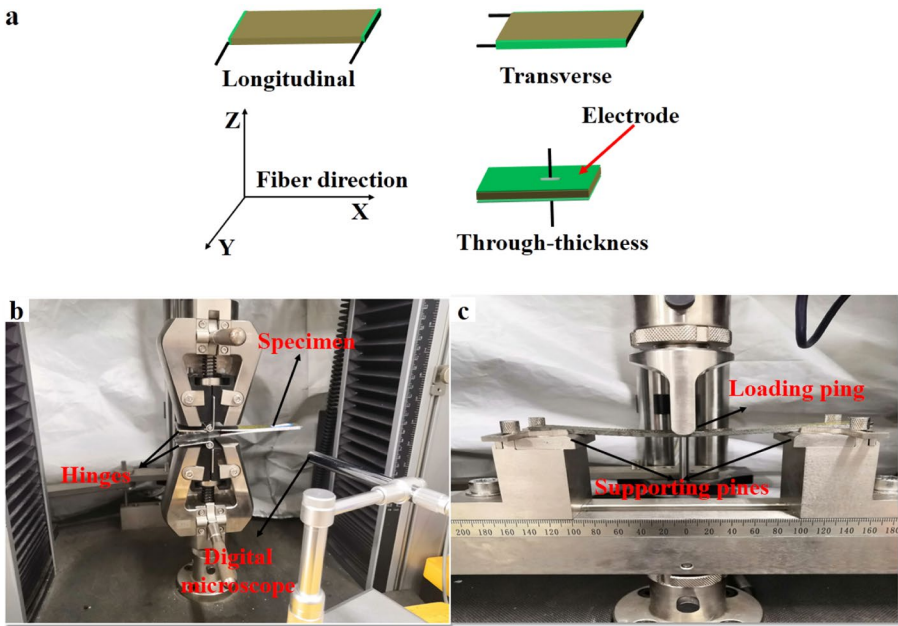
Fig. 4 (**a**) Conductivity testing, (**b**) Mode I test set-up and (**c**) Mode II test set-up

(SANS CMT4104) was used for this purpose. The number of specimens should be at least five in each group, and two hinges adhered to the pre-cracked end of each specimen. To visually observe the crack propagation and movement, white paint was applied to the surface of each specimen before testing and marked by vertical thin lines every 1 mm. To facilitate the observation of crack propagation, a digital microscope with maximum magnification of 500-times was placed in front of each sample. The total crack length (*a*) represented the sum of distance from the loading line to the endpoint from the inserted PTFE film plus the increase in crack growth. The tests were performed at 2 mm min^{-1} displacement control mode. The set-up of Mode I testing is displayed in Fig. 4b. The calculation of Mode I interlayer fracture toughness was carried out according to the compliance calibration (MCC) method (Eq. (2)):

$$G_{IC} = \frac{3P^2 C^{2/3}}{2A_1 bh} \qquad (2)$$

Where *P* is the load corresponding to the defined crack length (*a*). Compliance (*C*) represents the ratio of load point displacement to that corresponding to a defined crack length. *A$_1$* is the slope of the line on the least-squares plot of crack length normalized by specimen thickness (*a/h*) as a function of cube root of compliance (*C$^{1/3}$*). *h* and *b* are the thickness and width of the specimen.

1.1.8 Mode II Interlaminar Fracture Toughness Testing

Mode II interlaminar fracture toughness (G$_{IIC}$) testing of composite laminates was carried out according to standard ASTM D7905/D7905M. ENF test method was used to carry out

three-point bending tests on a universal testing machine. The experimental diagram of ENF testing is shown in Fig. 4c. Mode II interlaminar fracture toughness was measured by the compliance calibration (CC) method, including compliance calibration and fracture tests. The CC mark of pre-cracked area was made at the end of an inserted polytetrafluoroethylene (PTFE) film, in which a mark was made every 5 mm. A compliance calibration test was first performed at 20 mm and 40 mm from the crack tip, where fracture test point was 30 mm away from the crack tip (a_0). Meanwhile, the load versus displacement (P vs. δ) curve was recorded on the computer. Note that both CC and fracture tests were achieved using displacement-controlled loading at constant speed of 1 mm min^{-1}. To ensure experimental accuracy, at least 5 specimens were tested in each group. Data fitting of compliance versus crack length was carried out according to CC method (Eq. (3)):

$$C = A + ma^3 \tag{3}$$

Where C represents the compliance obtained from the slope of the linear region in δ-P curve drawn from two CC tests and one fracture test. A and m are CC coefficients, in which A represents the intercept and m is the slope obtained from the regression analysis.

Three compliance (C) values of the fitted straight line allowed the calculation of the cubic crack length of each test piece by linear least square calculation. The CC coefficients obtained from compliances versus crack length (C vs. a_0^3) are illustrated in Fig. 5.

The Mode II interlayer fracture toughness value was estimated through Eq. (4):
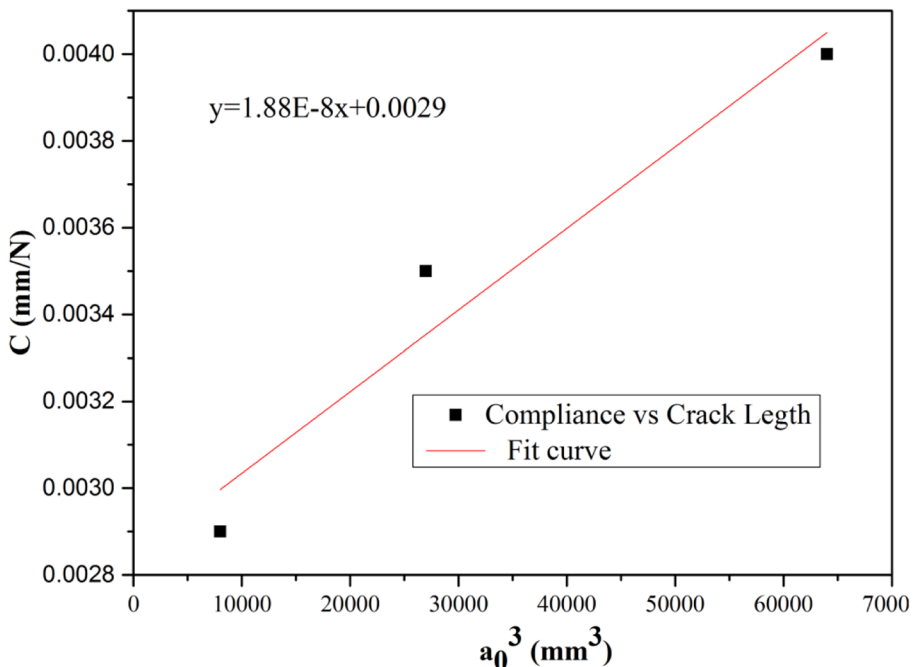
$$G_{IIC} = \frac{3mP^2 \max a_0^2}{2B} \tag{4}$$

Fig. 5 Method used for determining CC coefficients from compliances versus crack length (C vs. a_0^3)

Where P_{max} and a_0 are the maximum force generated in the fracture test and crack length used in fracture test, respectively. B represents the specimen width.

2 Results and Discussion

2.1 Conductivity of CTFs

In the first step, the electrical properties of PES films doped with MWCNTs were investigated. Figure 6 shows the conductivity and fitting curves of CTFs prepared with different contents of MWCNTs. Obviously, increased contents of MWCNTs led to enhanced electrical conductivity of the film. Since pure PES film was non-conductive, the introduction of 1 wt% MWCNTs yielded relatively high value of conductivity (21.3 S/m), which was many orders of magnitude higher than that of pure film. As MWCNTs contents further rose, the curve slowly enhanced then eventually flattened at MWCNTs content of 5 wt% at which conductivity reached 105 S/m. The conductivities of CTFs containing 10 and 15 wt% MWCNTs were recorded as 330.6 S/m and 484.2 S/m, respectively. To further analyze the conductive networks in CTFs, the classical statistical percolation theory (Eq. (5)) was used to fit the experimental data and the results are gathered in Fig. 6.

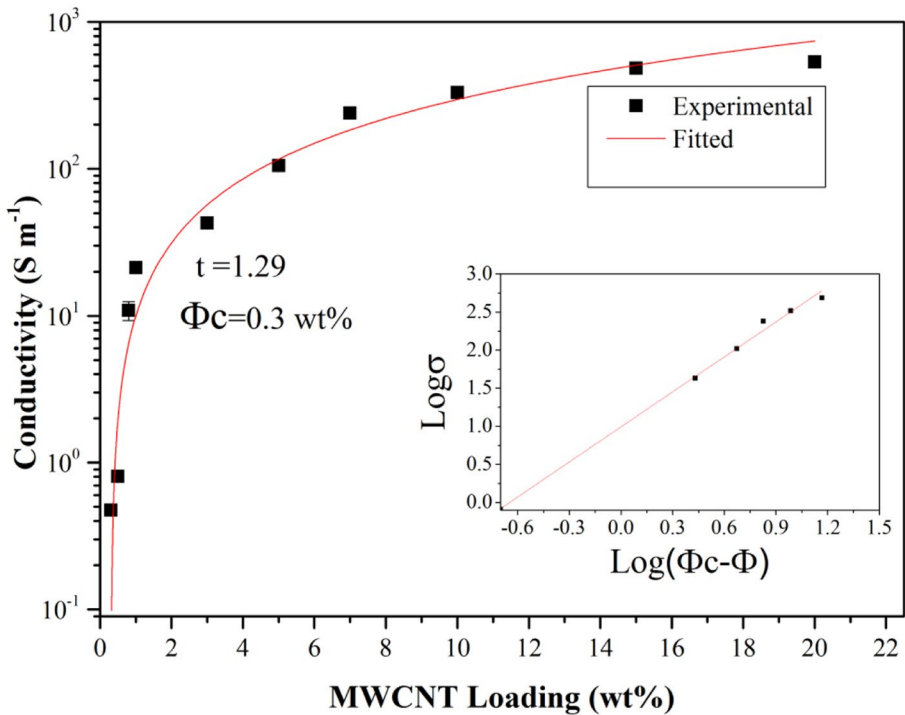$$\sigma = \sigma_0 \times (\Phi - \Phi c)^t \tag{5}$$

Fig. 6 Electrical conductivity of CTFs containing various loadings of MWCNTs. Inset shows log—log plot of conductivity versus Φ—Φ_C
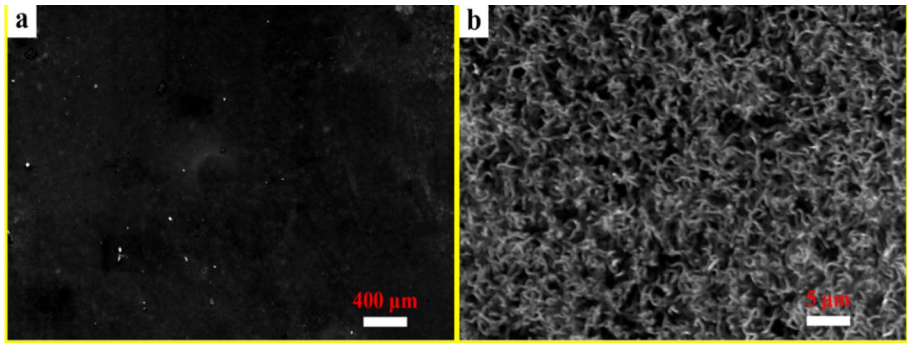
Fig. 7 SEM image of CTF containing 10 wt% MWCNTs

Where σ and σ_0 are the conductivity of CTF and nanofiller with different contents, respectively. Φ represents the nanofiller content, Φc is the critical concentration at percolation threshold, and t is the critical exponent depending on dimensionality of the conductive network [35].

t and Φ_c were obtained by fitting the experimental data through the least square method, in which σ and Φ were considered as independent variables. The fitting process consisted of gradually changing the z value in the logarithmic curve ($log\sigma \sim log\,(\Phi\text{-}\Phi_c)$) of conductivity and $log\,(\Phi\text{-}\Phi_c)$ until linear fitted curves with smallest errors were obtained. The fitted results (Fig. 6) suggested the critical filler concentration of the hybrid conductive film percolation at 0.3 wt%. The critical exponent (t) was estimated to 1.29. This value was low, thereby indicating the formation of complete conductive path in the film following 2D model [36].

A SEM image of CTF containing 10 wt% MWCNTs is provided in Fig. 7. At higher magnification (Fig. 7b), strong mechanical agitation and ultrasounds led to embedding of numerous curved and interlaced single MWCNTs in the matrix to form wavy shape. The interlaced MWCNTs first showed tree branch-like shape and then eventually transformed into mesh-like conductive network structure. Related literature suggested that more uniformly dispersed and loose CNTs would more likely be conductive to electron transfer [37, 38]. Therefore, an effective conductive network can be formed by introducing an appropriate amount of carbon nanotubes, which could increase the electrical conductivity. By contrast, much large or very low amounts MWCNTs would decline the conductivity.

3 Electrical Conductivity of CF/EP Composite Laminates

To explore the electrical properties of the composite laminates, four sets of specimens were made under the same conditions. To this end, the control sample and laminates interleaved by CTFs with MWCNTs loadings of 5, 10 and 15 wt% were tested. The changes in volume conductivity in all three different directions (fiber direction, Y-direction, and Z-direction) are presented in Fig. 8. The electrical conductivities of the above four sets of specimens in the fiber direction were measured as 1151.5 S/m, 1057.1 S/m, 1372.2 S/m and 1038.7 S/m, respectively. Besides, laminates interleaved by CTFs with MWCNTs loadings of 5 and 15 wt% showed slightly lower conductivities than those loaded with 10 wt% MWCNTs. Thus,
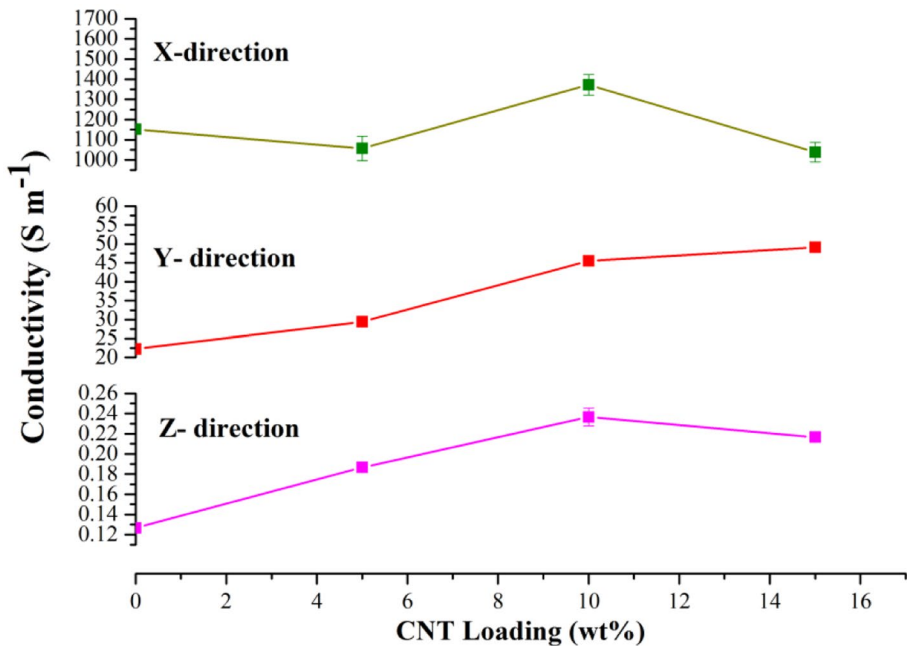
Fig. 8 Conductivities of composite samples in comparison with control sample (without interleaf). Conductivities obtained along the fiber direction (X-direction), transverse direction (Y-direction), and through-thickness direction (Z-direction) of composites interleaved with various MWCNTs loadings

low MWCNTs contents would form no effective conductive network path in the matrix. By contrast, very high contents MWCNTs would lead to serious agglomeration, thereby reducing the conductivity.

Similarly, the respective volume conductivities measured in Y-direction were 22.3 S / m, 29.4 S / m, 45.5 S / m, and 49.1 S / m. The increase in MWCNTs contents showed an initial raising trend. However, laminates interleaved by CTFs with MWCNTs loadings exceeding 10 wt% slowed down the upward trend until no major change was observed.

The respective volume conductivities along the Z-direction were estimated to 0.13 S / m, 0.19 S / m, 0.24 S / m, and 0.22 S / m. The change in conductivity was basically similar to that in Y-direction. Besides, conductivity displayed relatively large changes when compared to the control sample.

A low magnification SEM image of the composite laminate containing 10 wt% MWCNTs is shown in Fig. 9. Obvious traces of layering were observed, and both resin and conductive hybrid film were staggered to yield a relatively compact matrix structure. In large magnification images (Fig. 9b-d), MWCNTs tightly connected with the resin matrix in the film. Besides, some small gaps between the film and matrix existed (Fig. 9c-d). However, the resin still showed some filament-like connections with some MWCNTs. Thus, high temperature and hot pressing processes led to better fusing of the epoxy resin with the film, forming better conductive path and reducing the overall resistance of the resin.
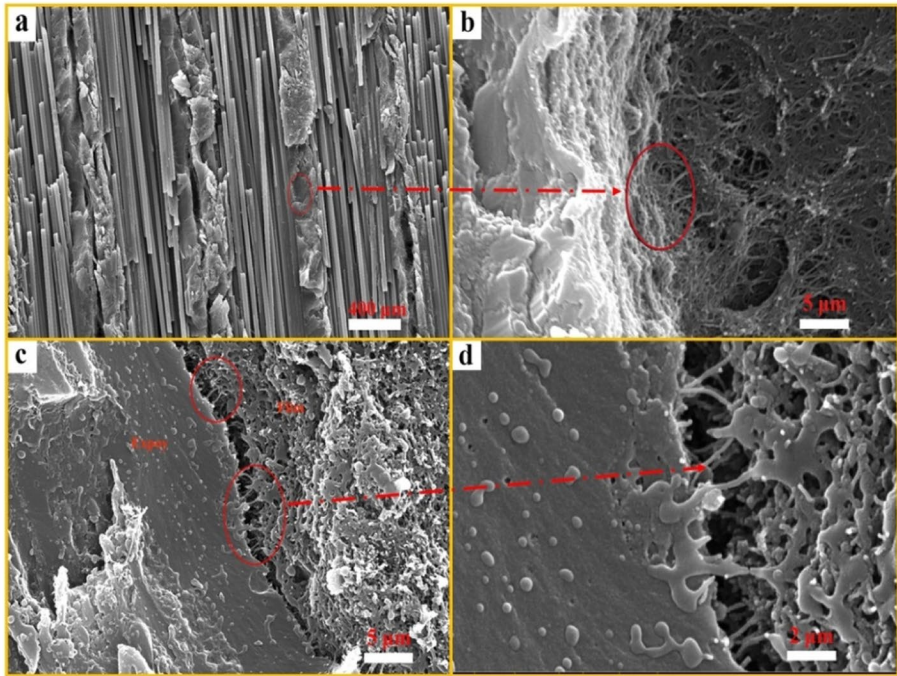
Fig. 9 SEM images of different sections of a 10% MWCNTs sample: (**a**) cross-section structure and (**b-d**) conductive networks formed via MWCNTs between the CTF and CF/EP

4 Mode I Interlaminar Fracture Toughness

Mode I interlaminar fracture toughness of control sample and laminates interleaved by CTFs with MWCNTs loadings of 5, 10, and 15 wt% were studied and the results were compared. Figure 10 shows the force-crack opening displacement curves for all composite laminate samples. During the initial stage of loading, the curve changed linearly until reaching a maximum force point, corresponding to crack initiation point. As crack continued to expand, the curve displayed a downward trend with over-all wavy pattern. The critical forces of all four groups of samples were estimated to 52.7 N, 66.0 N, 84.4 N and 65.64 N, respectively. Thus, the critical forces of the remaining three groups of samples increased when compared to the control sample. In particular, the critical force of composite laminate containing 10 wt% MWCNTs increased by 60.1%.

The variation in Mode I fracture toughness obtained by calculations versus crack propagation is displayed in Fig. 11. The fracture toughness values of all four different groups of samples showed a rapid increase during the initial stage followed by slowing down and eventually stabilizing. Furthermore, the increase in MWCNTs contents in composite laminates led to a decrease in fracture toughness. The reason for this may have to do with the inertness of MWCNTs surfaces, thereby weakening the interface interaction force between the hybrid film and CF/EP system. Besides, the increase in MWCNTs contents in the films induced local aggregation, generating
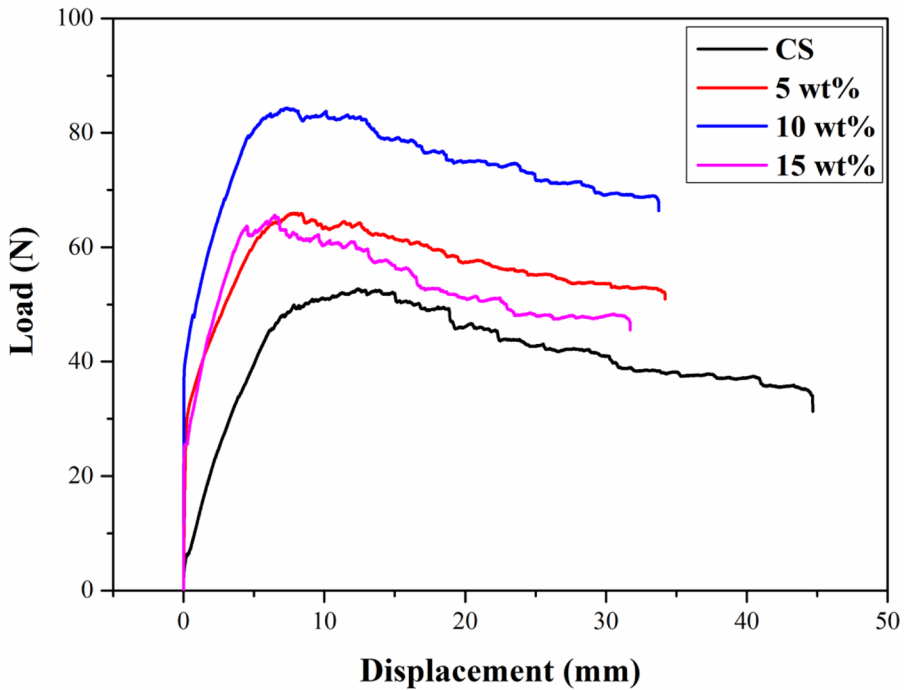
Fig. 10 Comparison of typical DCB load–displacement curves of composites with different interlayers

weak interfacial forces and reducing the interfacial compatibility between the film and epoxy.

The initial interlaminar fracture toughness (G_{IC}) and interlaminar fracture resistance (G_{IR}) of the composites are provided in Fig. 12. Note that G_{IC} represents the interlaminar fracture toughness at crack length of 50 mm, and G_{IR} is the average value of interlaminar fracture toughness at crack length of 60–80 mm. The trend in R-curves looked similar to that of load–displacement curves (Fig. 10). Also, the interlayer fracture toughness resistance (G_{IR}) specimen with inserted hybrid film was higher than that of control sample. For all samples, the toughness of composite laminates interleaved by CTFs with 10 wt% CNTs showed the highest values. The G_{IC} and G_{IR} of the latter specimen were estimated to 0.42 kJ/m^2 and 0.89 kJ/m^2, equivalent to 206% and 84% higher than those of control samples (0.14 kJ/m^2 and 0.48 kJ/m^2, respectively). The reason for this had to do with the good interface force between the matrix and interface when interleaving by CTFs with MWCNTs loading of 10 wt%. This led to uniform dispersion of MWCNTs, thereby improving the interface. On the other hand, laminates interleaved by CTFs with MWCNTs loading of 15 wt% showed smaller improvement in interfacial compatibility and forces by nanoparticles. Similarly, the agglomeration probability of carbon nanotubes between or around the interface of fiber-matrix was also high. Therefore, agglomeration of nanoparticles did not prevent delamination, leading to decreased interlayer fracture toughness.
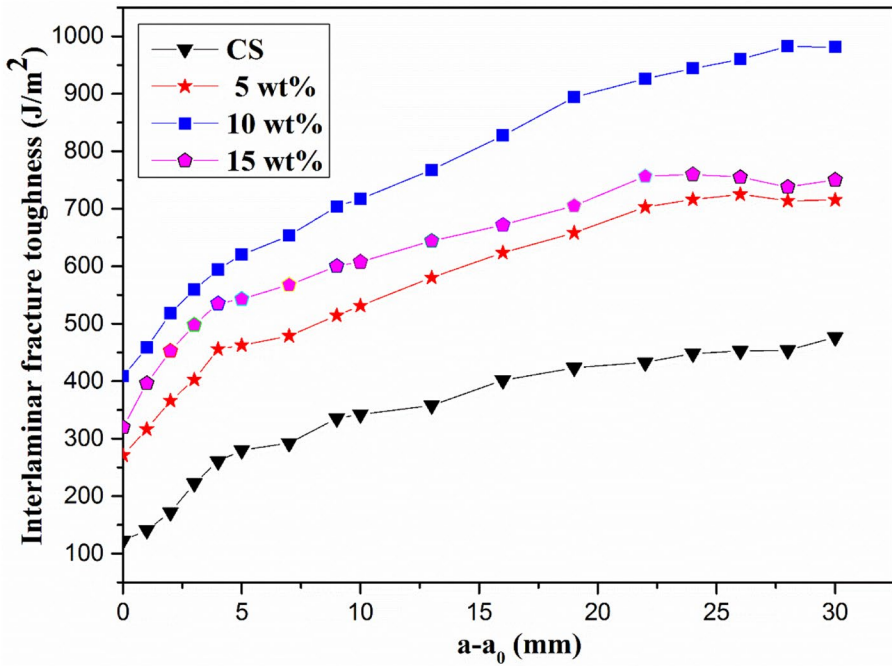
Fig. 11 Mode I fracture toughness-(a-a$_0$) curves obtained for composites with different interlayers

5 Mode II Interlaminar Fracture Toughness

The Mode II interlaminar fracture toughness tests were also carried out on all four groups of samples. Figure 13 shows a typical ENF test load–displacement curve, and Fig. 14 displays calculated values of mode II fracture toughness. Obviously, laminates interleaved by CTFs with MWCNTs loadings of 5, 10 and 15 wt% revealed significantly greater loading forces than control samples (Fig. 13).
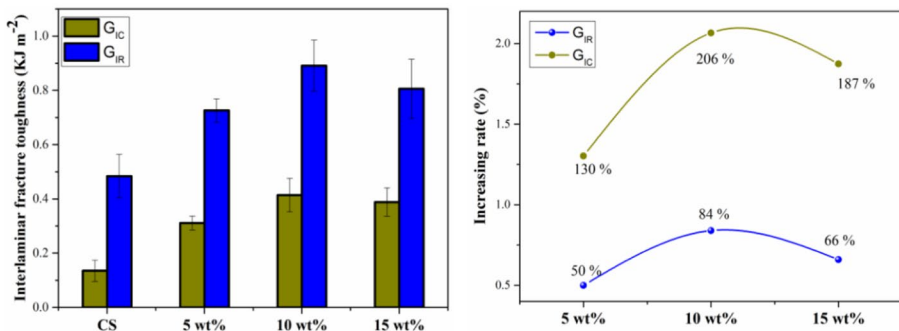

Fig. 12 Comparison of Mode I fracture toughness and resistance for composites containing various MWC-NTs loadings
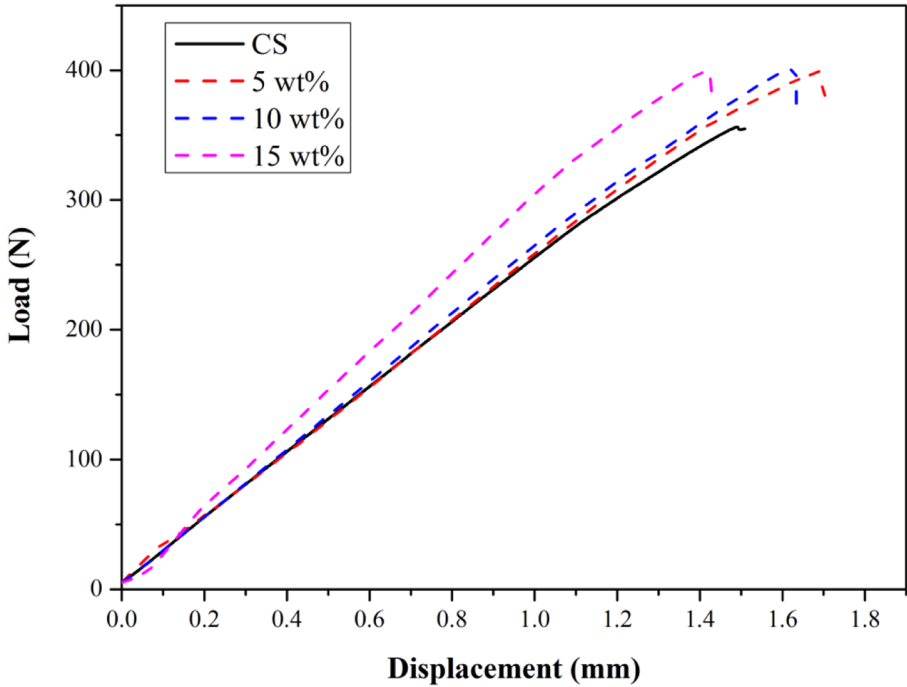
Fig. 13 Typical load–displacement curves obtained by ENF tests for composites with interlayers containing different MWCNTs loadings (5, 10, and 15 wt%)

Note that laminates interleaved by CTFs with MWCNTs loading of 10 wt% showed maximum force. Mode II fracture toughness improved in presence of hybrid films, and may also enhance the interface between the resin and matrix. The Mode II interlayer fracture toughness of control sample was estimated to 0.296 kJ/m^2 (Fig. 14). Laminates interleaved by CTFs with MWCNTs loading of 10 wt% displayed maximum enhancement of G_{IIC} (0.436 kJ/m^2) with a percentage improvement of 47%. Friction between the layer

Fig. 14 Mode II interlaminar fracture toughness (G_{IIC}) of composites laminates prepared with interlayers containing different MWCNTs loadings
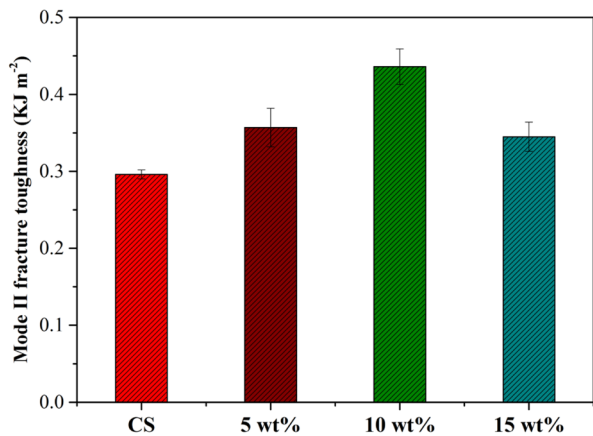
subjected to delamination and presence of hackles were the undelaying mechanisms behind
Mode II interlaminar fracture toughness [39]. The addition of nanohybrid film rendered
the interface of fiber-matrix rougher. This, in turn, led to better resistance to plastic defor-
mation caused by shear force and interlayer delamination. Therefore, the failure occurred
under greater shear force when compared to control sample. However, further increase in
MWCNTs content in intercalated film led to agglomeration in the matrix, thereby generat-
ing a local stress concentration point and damage under lower loads. Therefore, Mode II
interlaminar fracture toughness reduced for laminates interleaved by CTFs with MWCNTs
loadings above 10 wt%.

6 Fracture Toughness Mechanism

To analyze the effect of CTFs on interlaminar fracture mechanism, the fracture surface was
observed by SEM. Figure 15 presents SEM images of fractured surfaces of control sample
and laminates interleaved by CTFs with MWCNTs loading of 10 wt% under Mode I test-
ing conditions. The control sample displayed a delaminated surface with smooth interface
(Fig. 15(a, b)). Also, only a few resins adhered to the surface, indicating typical failure
mode of brittle fracture characteristics. The fibers could easily be pulled out of the matrix,
suggesting weak interface bonding.

Delaminated surface of laminates interleaved by CTFs with MWCNTs loading of 10
wt% is provided in Fig. 15(c-h). The low magnification image showed a very rough inter-
face (Fig. 15 (c, d)). Moreover, some convex torn small pieces of hybrid films adhered
to the matrix surface, significantly improving the fiber surface. The good interface force
between the film and epoxy matrix led to more absorption of fracture energy by the plas-
tic deformation of the film during stress. Meanwhile, the protruding part challenged crack
expansion, thereby deflecting and moving laterally. This, in turn, would consume more
energy to promote crack expansion and increase the interlaminar fracture toughness.

Higher magnification images of the interface between the film and epoxy matrix are
displayed in Fig. 15(e–h). Phase separation could be seen in Fig. 15(e, f). The fracture sur-
faces of the film and epoxy matrix presented irregular morphologies, and nanophase sepa-
ration structure formed during the curing of the epoxy resin. The phase separation structure
did not only maintain the mechanical properties of the matrix but also improve its tough-
ness [40].

In Fig. 15g, the matrix and MWCNTs looked very well combined. Besides, MWCNTs
were covered by the resin, and many were pulled out of the matrix. This led to the con-
sumption of more energy during the drawing process. MWCNTs subjected to drawing dis-
played bridging effect between the fiber and matrix, mechanically linking the interface.
The bridging effect improved the interlaminar fracture toughness by increasing the resist-
ance to crack growth.

SEM images of Mode II fractured surfaces of the control sample and laminates
interleaved by CTFs with MWCNTs loading of 10 wt% are shown in Fig. 16. Fiber
bundle exhibited small amounts of residual resin with smooth and flat fracture surface
of resin matrix (Fig. 16(a, b)), suggesting weak interface bonding between the car-
bon fiber and epoxy resin. The fracture surface of laminates interleaved by CTFs with
MWCNTs loading of 10wt% is provided in Fig. 16 (c, d). Compared to control sample,
the interface between the fiber and matrix obviously improved by becoming rough and
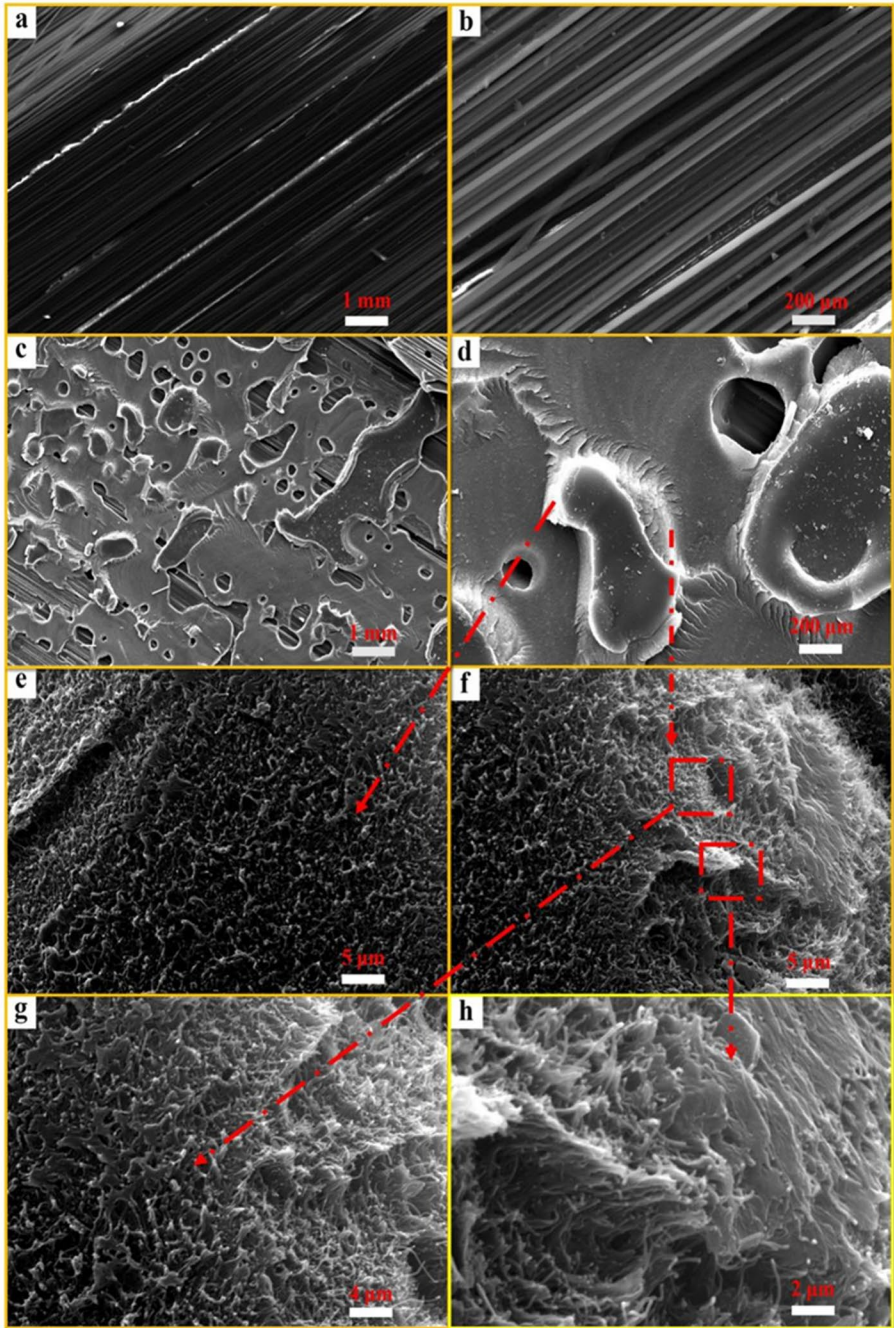uneven. The concave formation caused by fusion of the resin and matrix led to uneven

Fig. 15 SEM images of fracture surfaces: (**a, b**) control sample and (**c-h**) 10wt% MWCNTs/PES film intercalated laminate after DCB testing
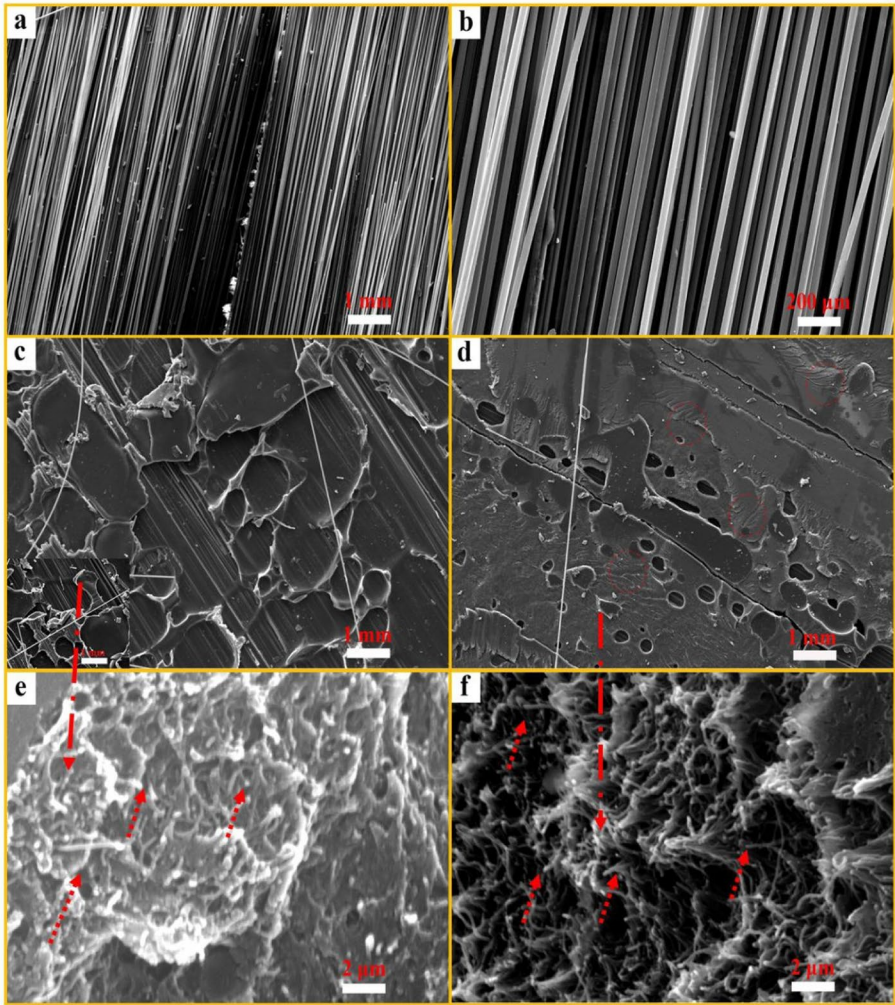
Fig. 16 SEM images of fracture surfaces: (**a,b**) control sample and (**c-f**) 10 wt% MWCNTs/PES film intercalated laminate sample after ENF test

interface. As a result, the hierarchical structure would resist crack growth and aggregation caused by shear force, thereby producing more resistance and consuming more energy. Also, hole-like structure with underneath fiber tow was observed in Fig. 16d. Thus, good interface was formed between the film and composite material. Many steps-like fracture surfaces and plastic fracture surfaces were also seen in hybrid film fragments. These fracture surfaces and plastic fracture surfaces would inhibit crack growth. During fracture process, the cracks in the interlaminar area forward in the zig-zag oblique direction, thereby increasing the path of cracks and consuming energy. Further expansion would require more energy and improve fracture toughness.

The high magnification images Fig. 16 (e, f) showed many pulled out and fractured MWCNTs. This, in turn, generated plastic deformation on the nearby interface, leading to better resistance to polymerization of microcracks. This made the final formation and transfer of cracks more difficult, thereby improving Mode II interlayer fracture toughness.

7 Conclusions

MWCNT/PES hybrid films were successfully prepared by solution casting method. The electrical properties of the as-obtained MWCNT/PES hybrid films were tested. The results showed that the electrical properties of MWCNT/PES hybrid films increased with loading amounts of MWCNTs. However, the change decreased for MWCNTs loadings above 10 wt%. CTFs were then inserted into the prepreg to prepare composite laminates, and their electrical and mechanical properties were tested. Compared to control sample, the electrical properties of composite samples with intercalation increased along the X, transverse (Y) and through-thickness (Z) directions at rates of 19%, 104% and 82.5%, respectively. The testing of the mechanical properties revealed Mode I fracture toughness (G_{IC}) reaching as high as 0.414 kJ/m^2, equivalent to 206% increase. Also, the highest value of fracture impedance (G_{IR}) was recorded as 0.891 kJ/m^2, equivalent to 84% increase. For Mode II interlaminar fracture toughness (G_{IIC}), the maximum value was estimated to 0.436 kJ/m^2, equivalent to 47% increase. The rise in fracture toughness was related to improvement in interface between CF/EP system, as well as enhancement in bonding force of the interface in presence of hybrid film. Thus, cracks expended more energy during interface growth, thereby improving the fracture toughness. In sum, these findings look promising for future fabrication of carbon fiber composite materials for the aerospace industry with simultaneously improved electrical and mechanical properties.

Compliance with Ethical Standard

Conflicts of interest The authors declared that they have no conflicts of interest to this work.

References

1. Katnam, K.B., Da Silva, L.F.M., Young, T.M.: Bonded repair of composite aircraft structures: A review of scientific challenges and opportunities. Prog. Aeronaut. Sci. **61**, 26–42 (2013). https://doi.org/10.1016/j.paerosci.2013.03.003
2. Kersiene, N., Raslavicius, L., Kersys, A., Kazys, R., Zukauskas, E.: Energo-Mechanical Evaluation of Damage Growth and Fracture Initiation in Aviation Composite Structures. Polym. Plast. Technol. Eng. **55**(11), 1137–1144 (2016). https://doi.org/10.1080/03602559.2015.1132452
3. Zhang, D., Ye, L., Deng, S., Zhang, J., Tang, Y., Chen, Y.: CF/EP composite laminates with carbon black and copper chloride for improved electrical conductivity and interlaminar fracture toughness. Compos. Sci. Technol. **72**(3), 412–420 (2012). https://doi.org/10.1016/j.compscitech.2011.12.002

Applied Composite Materials (2021) 28:17–37

4. Guo, M., Yi, X., Liu, G., Liu, L.: Simultaneously increasing the electrical conductivity and fracture toughness of carbon-fiber composites by using silver nanowires-loaded interleaves. Compos. Sci. Technol. **97**, 27–33 (2014). https://doi.org/10.1016/j.compscitech.2014.03.020

5. Guo, M., Yi, X.: The production of tough, electrically conductive carbon fiber composite laminates for use in airframes. Carbon **58**, 241–244 (2013). https://doi.org/10.1016/j.carbon.2013.02.052

6. Li, Y., Zhang, H., Porwal, H., Huang, Z., Bilotti, E., Peijs, T.: Mechanical, electrical and thermal properties of in-situ exfoliated graphene/epoxy nanocomposites. Compos. Part A: Appl. Sci. **95**, 229–236 (2017). https://doi.org/10.1016/j.compositesa.2017.01.007

7. Garcia, E.J., Wardle, B.L., Hart, A.J., Yamamoto, N.: Fabrication and multifunctional properties of a hybrid laminate with aligned carbon nanotubes grown In Situ. Compos. Sci. Technol. **68**(9), 2034–2041 (2008). https://doi.org/10.1016/j.compscitech.2008.02.028

8. Thostenson, E., Ren, Z., Chou, T.-W.: Advances in the Science and Technology of Carbon Nanotubes and Their Composites: A Review. Compos. Sci. Technol. **61**(13), 1899–1912 (2001). https://doi.org/10.1016/S0266-3538(01)00094-X

9. Xiang, D., Wang, L., Tang, Y., Zhao, C., Harkin-Jones, E., Li, Y.: Effect of phase transitions on the electrical properties of polymer/carbon nanotube and polymer/graphene nanoplatelet composites with different conductive network structures. Polym. Int. **67**(2), 227–235 (2018). https://doi.org/10.1002/pi.5502

10. Xiang, D., Guo, J., Kumar, A., Chen, B., Harkin-Jones, E.: Effect of processing conditions on the structure, electrical and mechanical properties of melt mixed high density polyethylene/multiwalled CNT composites in compression molding. Mater. Test. **59**(2), 136–147 (2017). https://doi.org/10.3139/120.110974

11. Chou, T.-W., Gao, L., Thostenson, E.T., Zhang, Z., Byun, J.-H.: An assessment of the science and technology of carbon nanotube-based fibers and composites. Compos. Sci. Technol. **70**(1), 1–19 (2010). https://doi.org/10.1016/j.compscitech.2009.10.004

12. Kim, Y., Shin, T., Choi, H., Kwon, J., Chung, Y.-C., Yoon, H.: Electrical conductivity of chemically modified multiwalled carbon nanotube/epoxy composites. Carbon **43**, 23–30 (2005). https://doi.org/10.1016/j.carbon.2004.08.015

13. Garnier, C., Pastor, M.-L., Eyma, F., Lorrain, B.: The detection of aeronautical defects in situ on composite structures using Non Destructive Testing. Compos. Struct. **93**(5), 1328–1336 (2011). https://doi.org/10.1016/j.compstruct.2010.10.017

14. Baker, A., Gunnion, A.J., Wang, J.: On the Certification of Bonded Repairs to Primary Composite Aircraft Components. J. Adhes. **91**(1–2), 4–38 (2015). https://doi.org/10.1080/00218464.2014.883315

15. Kostopoulos, V., Baltopoulos, A., Karapappas, P., Vavouliotis, A., Paipetis, A.: Impact and after-impact properties of carbon fibre reinforced composites enhanced with multi-wall carbon nanotubes. Compos. Sci. Technol. **70**(4), 553–563 (2010). https://doi.org/10.1016/j.compscitech.2009.11.023

16. Garg, A.C.: Delamination—a damage mode in composite structures. Eng. Fract. Mech. **29**(5), 557–584 (1988). https://doi.org/10.1016/0013-7944(88)90181-6

17. Sela, N., Ishai, O.: Interlaminar fracture toughness and toughening of laminated composite materials: a review. Compos. **20**(5), 423–435 (1989). https://doi.org/10.1016/0010-4361(89)90211-5

18. Hojo, M., Ando, T., Tanaka, M., Adachi, T., Shojiro, O., Endo, Y.: Modes I and II interlaminar fracture toughness and fatigue delamination of CF/epoxy laminates with self-same epoxy interleaf. Int. J. Fatigue. **28**(10), 1154–1165 (2006). https://doi.org/10.1016/j.ijfatigue.2006.02.004

19. Yan, W., Liu, H.-Y., Mai, Y.W.: Numerical study on the mode I delamination toughness of Z-pinned laminates. Compos. Sci. Technol. **63**(10), 1481–1493 (2003). https://doi.org/10.1016/S0266-3538(03)00167-2

20. Jain, L., Mai, Y.W.: Determination of mode II delamination toughness of stitched laminated composites. Compos. Sci. Technol. **55**(3), 241–253 (1995). https://doi.org/10.1016/0266-3538(95)00089-5

21. Tanzawa, Y., Watanabe, N., Ishikawa, T.: Interlaminar fracture toughness of 3-D orthogonal interlocked fabric composites. Compos. Sci. Technol. **59**, 1261–1270 (1999). https://doi.org/10.1016/S0266-3538(98)00167-5

22. Dransfield, K., Baillie, C., Mai, Y.W.: Improving the delamination resistance of CFRP by stitching—a review. Compos. Sci. Technol. **50**(3), 305–317 (1994). https://doi.org/10.1016/0266-3538(94)90019-1

23. Narducci, F., Pinho, S.T.: Interaction between nacre-like CFRP mesolayers and long-fibre interlayers. Compos. Struct. **200**, 921–928 (2018). https://doi.org/10.1016/j.compstruct.2018.05.103

24. Li, W., Xiang, D., Wang, L., Harkin-Jones, E., Zhao, C., Wang, B., Li, Y.: Simultaneous enhancement of electrical conductivity and interlaminar fracture toughness of carbon fiber/epoxy

composites using plasma-treated conductive thermoplastic film interleaves. RSC. Adv. **8**(47), 26910–26921 (2018). https://doi.org/10.1039/c8ra05366a

25. Palazzetti, R., Zucchelli, A., Gualandi, C., Focarete, M.L., Donati, L., Minak, G., Ramakrishna, S.: Influence of electrospun Nylon 6,6 nanofibrous mats on the interlaminar properties of Gr-epoxy composite laminates. Compos. Struct. **94**(2), 571–579 (2012). https://doi.org/10.1016/j.compstruct.2011.08.019

26. Guo, M., Yi, X., Rudd, C., Liu, X.: Preparation of highly electrically conductive carbon-fiber composites with high interlaminar fracture toughness by using silver-plated interleaves. Compos. Sci. Technol. **176**, 29–36 (2019). https://doi.org/10.1016/j.compscitech.2019.03.014

27. Zheng, W., Yao, Z., Lin, H., Zhou, J., Cai, H., Qi, T.: Improved fracture toughness of carbon fiber fabric/epoxy composite laminates using polyether sulfone fibers. High Perform. Polym. **31**(8), 996–1005 (2019). https://doi.org/10.1177/0954008318812151

28. Xu, H., Tong, X., Zhang, Y., Li, Q., Lu, W.: Mechanical and electrical properties of laminated composites containing continuous carbon nanotube film interleaves. Compos. Sci. Technol. **127**, 113–118 (2016). https://doi.org/10.1016/j.compscitech.2016.02.032

29. Yu, Y., Zhang, Z., Gan, W., Wang, M., Li, S.: Effect of Polyethersulfone on the Mechanical and Rheological Properties of Polyetherimide-Modified Epoxy Systems. Ind. Eng. Chem. Res. **42**(14), 3250–3256 (2003). https://doi.org/10.1021/ie0210309

30. Rajasekaran, R., Alagar, M., Chozhan, C.K.: Effect of polyethersulfone and N, N ’-bismaleimido-4,4 ’-diphenyl methane on the mechanical and thermal properties of epoxy systems. Express Polym. Lett. **2**(5), 339–348 (2008). https://doi.org/10.3144/expresspolymlett.2008.40

31. Ying, W.B., Yang, H.S., Moon, D.S., Lee, M.W., Ko, N.Y., Kwak, N.H., Lee, B., Zhu, J., Zhang, R.: Epoxy resins toughened with in situ azide-alkyne polymerized polysulfones. J. Appl. Polym. Sci. **135**(5) (2018). https://doi.org/https://doi.org/10.1002/app.45790

32. Lee, S.-E., Jeong, E., Lee, M.Y., Lee, M.-K., Lee, Y.-S.: Improvement of the mechanical and thermal properties of polyethersulfone-modified epoxy composites. J. Ind. Eng. Chem. **33**, 73–79 (2016). https://doi.org/10.1016/j.jiec.2015.09.022

33. Mimura, K., Ito, H., Fujioka, H.: Improvement of thermal and mechanical properties by control of morphologies in PES-modified epoxy resins. Polymer **41**(12), 4451–4459 (2000). https://doi.org/10.1016/S0032-3861(99)00700-4

34. Cheng, C., Chen, Z., Huang, Z., Zhang, C., Tusiime, R., Zhou, J., Sun, Z., Liu, Y., Yu, M., Zhang, H.: Simultaneously improving mode I and mode II fracture toughness of the carbon fiber/epoxy composite laminates via interleaved with uniformly aligned PES fiber webs. Compos. Part A: Appl. Sci. **129** (2020). https://doi.org/https://doi.org/10.1016/j.compositesa.2019.105696

35. Bauhofer, W., Kovacs, J.Z.: A review and analysis of electrical percolation in carbon nanotube polymer composites. Compos. Sci. Technol. **69**(10), 1486–1498 (2009). https://doi.org/10.1016/j.compscitech.2008.06.018

36. Breton, Y., Désarmot, G., Salvetat, J.-P., Delpeux, S., Sinturel, C., Beguin, F., Bonnamy, S.: Mechanical properties of multiwall carbon nanotubes/epoxy composites: Influence of network morphology. Carbon **42**, 1027–1030 (2004). https://doi.org/10.1016/j.carbon.2003.12.026

37. Kobashi, K., Ata, S., Yamada, T., Futaba, D.N., Yumura, M., Hata, K.: A dispersion strategy: dendritic carbon nanotube network dispersion for advanced composites. Chem. Sci. **4**(2), 727–733 (2013). https://doi.org/10.1039/c2sc21266h

38. Wong, D.W.Y., Lin, L., Mcgrail, P.T., Peijs, T., Hogg, P.J.: Improved fracture toughness of carbon fibre/epoxy composite laminates using dissolvable thermoplastic fibres. Compos. Part A: Appl. Sci. **41**(6), 759–767 (2010). https://doi.org/10.1016/j.compositesa.2010.02.008

39. Seyhan, A.T., Tanoglu, M., Schulte, K.: Mode I and mode II fracture toughness of E-glass non-crimp fabric/carbon nanotube (CNT) modified polymer based composites. Eng. Fract. Mech. **75**(18), 5151–5162 (2008). https://doi.org/10.1016/j.engfracmech.2008.08.003

40. Guo, J., Zhang, Q., Gao, L., Zhong, W., Sui, G., Yang, X.: Significantly improved electrical and interlaminar mechanical properties of carbon fiber laminated composites by using special carbon nanotube pre-dispersion mixture. Compos. Part A: Appl. Sci. **95**, 294–303 (2017). https://doi.org/10.1016/j.compositesa.2017.01.021